Applied Catalysis B: Environmental 203 (2017): 591 - 598

DOI: http://dx.doi.org/10.1016/j.apcatb.2016.10.062

Exploring the role of the catalytic support sorption capacity on the hydrodechlorination kinetics by the use of carbide-derived carbons

*Macarena Munoz[1], Gui-Rong Zhang[2] and Bastian J.M. Etzold[1,2]**

[1]*Lehrstuhl für Chemische Reaktionstechnik, Friedrich-Alexander-Universität Erlangen-Nürnberg, Egerlandstrasse 3, 91058 Erlangen, Germany*

[2]*Ernst-Berl-Institut für Technische und Makromolekulare Chemie, Technische Universität Darmstadt, Alarich-Weiss-Srasse 8, 6428 Darmstadt, Germany*

*Corresponding author: Prof. Bastian J.M. Etzold

Tel.: +49 (6151) 1629983

Fax: +49 (6151) 1629982

E-mail: etzold@tc1.tu-darmstadt.de

Keywords: Catalytic hydrodechlorination; adsorption; carbide-derived carbon; Pd; 4-chlorophenol.

Abstract

This work aims at evaluating the effect of the catalytic support sorption capacity on the hydrodechlorination (HDC) process. Carbide-derived carbons (CDCs) have been selected for such goal as their high purity and tunable pore structure makes them a suitable carbon model material. CDCs were synthesized from TiC by chlorination at different extraction temperatures (800 – 1300 ºC) in order to selectively modify their pore structure and crystallinity. Afterwards, the catalysts were produced using a three step process of sulfuric acid treatment, ion-adsorption of palladium precursor and gas phase reduction. Pd/TiC-CDC (1% wt.) catalysts were tested in the HDC of 4-chlorophenol (4-CP) in both aqueous and organic phases under ambient conditions (30 ºC, 1 atm, $[4\text{-CP}]_0$ = 2.9 mmol L^{-1}, [Pd-TiC-CDC] = 1 g L^{-1}, 50 N mL H_2 min^{-1}). The experimental results were successfully fitted by an expanded kinetic model which accounts for consecutive reaction and sorption processes in parallel, allowing to deduce true HDC kinetic constants.

The sorption capacity of the support was found to determine the HDC rates in aqueous phase. In this sense, those catalysts showing the highest surface areas and lowered ordered structures led to higher HDC rates, confirming that a high surface density of 4-CP onto the catalyst surface enhances significantly the HDC reaction. The optimum catalyst (Pd/TiC-CDC-1000) led to the complete conversion of 4-CP in 15 min at a HDC rate of 4.1 x 10^{-2} L s^{-1} g_{cat}^{-1}.

1. Introduction

The generation of industrial wastewaters has become a problem of increasing concern within the past decades. Particular attention is receiving the discharge of organochlorinated pollutants, highly toxic species for which the environment has low assimilative capacity. These xenobiotic compounds are quite relevant in industry nowadays due to their antimicrobial properties, which make them attractive for the production of herbicides, fungicides, insecticides or broad antibacterial agents [1]. Consequently, their presence in the aquatic environment has inevitably increased during the past few decades [2-5], involving serious implications for both the environment and public health. Since the generation of these hazardous effluents is in most cases unavoidable, the development of cost-efficient and sustainable processes for organochlorinated pollutants remediation is imperative. In this context, much scientific effort has been put into investigation of catalytic hydrodechlorination (HDC) as a promising alternative to the broadly established conventional methods [6].

Most HDC studies have focused on the active phase and thus, a number of metals such as Pd, Pt, Ni, Cu and Rh have been tested [7-14]. Among them, Pd has been widely accepted by the scientific community as the most effective metal due to its inherent capacity to dissociate hydrogen and promote C-Cl bond scission as well as to its high resistance to the poisoning properties of the chloride ions released during reaction [1, 6, 15]. Although to a lesser extent, catalytic supports have been also investigated as they play an important role in the activity, selectivity and stability of the catalyst. Inorganic supports such as aluminum- or silicon oxides have been widely employed [8, 12, 16], but carbonaceous materials and, in particular, activated carbon (AC) are the most frequently used because of their chemical resistance, high surface area and relatively inexpensiveness [1, 17-20]. Moreover, their surface chemistry can be appropriately adapted to the reaction demands through activation processes [21, 22] although this aspect has not been deeply explored for the HDC reaction. In any case, the effect of functional groups has been mainly related to the dispersion of the active phase [18, 22]. For instance, Calvo et al. [18] showed that the presence of carboxylic and lactone groups in Pd/AC catalysts led to

enhanced conversion of 4-CP and improved selectivity to cyclohexanol due to a more homogeneous dispersion of the active phase.

Despite its high importance, studying support influences of porous carbons is challenging as for AC the production leads to scattering material properties due to the diverse quality of the raw material (e.g. wood, coal or fruit stones) [23-25]. As a result, performance of catalysts supported on AC can vary strongly. In a recent contribution, we demonstrated that sorption of reaction species, which is mainly related to the properties of the catalytic support, plays a key role on the HDC kinetics dealing with AC-supported catalysts and must be considered to deduce true kinetic constants for the HDC process [26]. Including the sorption processes in an expanded kinetic model resulted in a reasonable fit with both negligible and high adsorption capacity catalysts (Pd/Al_2O_3 and Pd/AC, respectively). Nevertheless, although different commercial Pd/AC catalysts were tested, the role of the textural properties and the crystallinity of the carbon support on the HDC performance remain unclear.

In this context, carbide-derived carbons (CDCs) appear as promising model catalyst supports to study support influence for HDC reactions. CDCs are formed by selective extraction of the metal or metalloid atoms, transforming the carbide structure into pure carbon but maintaining the original shape and volume of the precursor. The resulting carbon structure depends in high reproducibility on the synthesis method, applied temperature, pressure and choice of carbide precursor. In this sense, the pore structure can be accurately tuned ranging from ultramicroporous to mesoporous and from extremely disordered to crystalline structures [27-31]. The applicability of CDC as metal noble support in catalysis has been already demonstrated [32-36] but its application in HDC has not been investigated in the literature so far.

In this work, we explore the role of the sorption capacity of the catalytic support on the HDC kinetics by using well-defined CDCs. These materials were synthesized from titanium carbide at different temperatures in order to vary their textural properties and degree of structural order. Pd was used as active phase due to its outstanding role in HDC [6]. Prior their deposition, CDCs were oxidized in sulfuric acid medium to introduce functional groups providing surface charges and breaking the

hydrophobic character [27]. The resulting Pd/TiC-CDC catalysts prepared by ion-exchange were tested in the HDC of 4-chlorophenol (4-CP) in both aqueous and organic (isopropanol) phases.

2. Materials and methods

2.1. Preparation of the Pd/TiC-CDC catalysts

The TiC-CDC supports were synthesized using titanium carbide (TiC, 99.5% purity, 2 μm diameter, Alfa Aesar GmbH & Co KG) as precursor following a reported methodology [30, 33]. Briefly, the TiC powder was subjected to chlorination in an alumina tubular reactor, lined by thin graphite foil, at different temperatures (800, 1000, 1200 and 1300 °C) using a mixture of Cl_2 and He (C_{Cl2} = 1 mol m^{-3}, reactor diameter 3.2 cm, superficial velocity of 3 cm s^{-1}). After 5 h the chlorination was stopped by purging with He for 30 min. A hydrogenation post-synthesis treatment (30 min) was then carried out at a temperature equal to the CDC synthesis one to remove residual chlorine and metal chlorides from the pores of the carbon support, obtaining a hydrogen-terminated surface. Typically 5 g of carbide were completely converted to 1 g of TiC-CDC. Materials are denoted according to their chlorination temperature as TiC-CDC-T.

Prior to Pd impregnation, the TiC-CDC supports were functionalized with 50 wt.% H_2SO_4 at 90 °C for 2 h using 50 mL acid per 1 g TiC-CDC. After the treatment, the samples were washed with large amount of distilled water until neutrality and dried overnight at 60 °C.

The deposition of Pd onto the TiC-CDC solids was performed with an ion–adsorption method where the volume of precursor solution exceeds the pore volume of the carbon support. The ratio of solution to carbon was adjusted to 50 $mL_{solution}$ $g_{TiC\text{-}CDC}^{-1}$. An aqueous solution of $PdCl_2$ (pH = 1) was used as precursor, adjusting the Pd load in the catalyst to a nominal 1 wt.%. The suspension was stirred at room temperature for 24 h. Afterwards the resulting Pd/TiC-CDC catalyst was filtered and washed with 200 mL water (per gram of catalyst) of the same pH as the impregnation solution and dried subsequently at

60 °C overnight. Finally, the catalysts (0.5 g) were reduced for 2 h at 150 °C with 10 L_N h^{-1} of 30 vol.% H_2 in N_2 in a tubular quartz glass reactor with an inner diameter of 3.2 cm.

2.2. Catalyst characterization

The porous structure of the catalysts was characterized from nitrogen adsorption-desorption at 77 K with a Quantachrome Quadrasorb SI apparatus. The software QuadraWin version 5.02 was employed for subsequent data evaluation using Quenched Solid Density Functional Theory (QSDFT) for slit/cylindrical pores. The mean pore size (MPS) was determined assuming slit pores with the specific pore volume (SPV) and the specific surface area (SSA) calculated with QSDFT from N_2-sorption: MPS = 2·SPV/SSA.

Palladium contents were determined by inductively coupled plasma (ICP-AES, PerkinElmer Plasma 400) after digestion of the samples with a mixture of concentrated HF, HNO_3 and HCl solution in the proportion of 4:1:1. Powder X-ray diffraction (XRD) patterns were recorded in a Philips X'Pert Pro MPD diffractometer operated at 40 kV and 40 mA using Cu $k\alpha$ radiation in the 2θ range from 10 to 80º (steps: 0.02º, 30s per step). Raman spectra were recorded in a Horiba Jobin Ybon HR 800 spectrometer using a HeNe laser operating at 633 nm with a power of 20 mW.

The dispersion of Pd on the TiC-CDC supports was determined by measuring the charges (Q_{CO}) associated with electrooxidation (stripping) of adsorbed CO on Pd at saturated coverage. The adsorption of CO was carried out at a constant electrode potential of 0.05 V vs RHE by bubbling CO gas through the electrolyte for 15 min. Subsequently, the remained unadsorbed CO was purged by flowing high purity N_2 for another 15 min. The CO-stripping curves were recorded in 0.5 M H_2SO_4 solution at a scanning rate of 20 mV s^{-1}. The CO-stripping signals were corrected by subtracting the background currents associating with double layer charging and surface oxidation, which were measured in the

subsequent anodic scan voltammetry. Given the well-established CO adsorption stoichiometry on a Pd surface (CO: Pd = 1:1), the dispersion can be calculated using the following equation:

$$D = \frac{\frac{Q_{CO}}{Q_e}}{2\frac{W_{Pd}NA}{M_{Pd}}} \quad (1)$$

where Q_e is the elementary charge (1.602×10^{-19} C); W_{Pd} is the actual loading of Pd on the electrode; NA is the Avogadro constant (6.02×10^{23} mol^{-1}); M_{Pd} is the molar weight of Pd (106.42 g mol^{-1}).

2.3. Typical reaction procedure

HDC runs were carried out during 3 h in a glass slurry-type reactor (250 mL), equipped with H_2 supply, a magnetic stirrer (750 rpm) and temperature control. In a typical experiment, 140 mL of 4-CP aqueous solution (2.9 mmol L^{-1} initial concentration) were placed in the reactor and heated to the desired temperature (20, 30 or 40 °C). Once the temperature was reached the reaction was started by introducing the catalyst (1 g L^{-1}) and feeding H_2 at a flow rate of 50 NmL min^{-1}. The solid catalyst was previously suspended in 10 mL of water and the solution was sonicated for 15 min. Blank tests in absence of catalyst at all the temperatures tested confirmed that not reaction proceeds after 3 h. Additional experiments were also carried out using isopropanol as matrix for the reaction. In this case, HDC runs were performed with a 4-CP concentration of 0.78 mmol L^{-1}, whereas catalyst concentration and H_2 flow were the same previously mentioned. The existence of both internal and external mass transfer limitations under these operating conditions was discarded according to our previous work [26].

Equilibrium adsorption tests with the CDC-based catalysts were performed under the same operating conditions and procedure as the HDC runs but in the absence of hydrogen. Solutions of the target pollutant (4-CP) and the main reaction product (phenol, Ph) were prepared with concentrations from 0 to 10 mmol L^{-1}. The equilibration time was 1 h for all the samples. Subsequent analysis of the equilibrium data was carried out using the Langmuir equation.

The HDC data were fitted by an expanded kinetic model which accounts for both the consecutive reaction and adsorption processes in parallel [26]. Model simulations were performed using the kinetic modelling software package Presto-kinetics version 7.2.2. Pseudo-first order approaches are used for the consecutive HDC steps whereas the parallel sorption processes are implemented according to the Langmuir assumptions. It is assumed that adsorption takes place mainly on the TiC-CDC support [37]. The net production rates of the species involved in reaction can be expressed as follows (Eqs. 2-7):

$$\frac{C_{4-CP\ FREE}}{dt_{mod}} = -k_{HDC-1} \cdot C_{4-CP\ FREE} - k_{ADS-1} \cdot C_{4-CP\ FREE} \cdot L + \frac{k_{ADS-1} \cdot C_{4-CP\ ADS}}{K_{SORP-4-CP}} \quad (2)$$

$$\frac{dC_{4-CP\ ADS}}{dt_{mod}} = k_{ADS-1} \cdot C_{4-CP\ FREE} \cdot L - \frac{k_{ADS-1} \cdot C_{4-CP\ ADS}}{K_{SORP-4-CP}} \quad (3)$$

$$\frac{dL}{dt_{mod}} = -k_{ADS-1} \cdot C_{4-CP\ FREE} \cdot L + \frac{k_{ADS-1} \cdot C_{4-CP\ ADS}}{K_{SORP-4-CP}} - k_{ADS-2} \cdot C_{Ph\ FREE} \cdot L + \frac{k_{ADS-2} \cdot C_{Ph\ ADS}}{K_{SORP-Ph}} \quad (4)$$

$$\frac{dC_{Ph\ FREE}}{dt_{mod}} = k_{HDC-1} \cdot C_{4-CP\ FREE} - k_{HDC-2} \cdot C_{Ph\ FREE} - k_{ADS-2} \cdot C_{Ph\ FREE} \cdot L + \frac{k_{ADS-2} \cdot C_{Ph\ ADS}}{K_{SORP-Ph}} \quad (5)$$

$$\frac{dC_{Ph\ ADS}}{dt_{mod}} = k_{ADS-2} \cdot C_{Ph\ FREE} \cdot L - \frac{k_{ADS-2} \cdot C_{Ph\ ADS}}{K_{SORP-Ph}} \quad (6)$$

$$\frac{dC_{C-one\ FREE}}{dt_{mod}} = k_{HDC-2} \cdot C_{Ph\ FREE} \quad (7)$$

where $C_{4\text{-CP FREE}}$, $C_{\text{Ph FREE}}$ and $C_{\text{C-one FREE}}$ are the concentrations of 4-CP, Ph and cyclohexanone (C-one) free in solution; $C_{4\text{-CP ADS}}$ and $C_{\text{Ph ADS}}$ are the concentrations of 4-CP and Ph adsorbed onto the TiC-CDC support; $k_{\text{HDC-1}}$ and $k_{\text{HDC-2}}$ are the HDC apparent first order rate constants of each HDC reaction step shown in Scheme 1; $k_{\text{ADS-1}}$ and $k_{\text{ADS-2}}$ are the adsorption rate constants of 4-CP, Ph and C-one; $K_{\text{SORP-4-CP}}$ and $K_{\text{SORP-Ph}}$ are the Langmuir adsorption equilibrium constants previously calculated in the adsorption equilibrium experiments for 4-CP and Ph; and L represents the amount of free sites present in the TiC-CDC support, whose initial value corresponds to the maximum adsorbed concentration ($C_{\text{ADS-MAX}}$), calculated in the adsorption equilibrium experiments as well.

To be able to compare the HDC rate constants taking into account the Pd dispersion of the catalysts, the modified reaction time t_{mod} was used. It is defined as the product of time and concentration of Pd on the catalyst surface as follows:

$$t_{mod} = t\frac{m_{Pd\ surf}}{V} \quad (8)$$

The evolution of the HDC/adsorption runs was carried out by periodically withdrawing and analysing liquid samples from the reactor. Once the samples were filtered (PTFE filter, 0.2 μm), they were analysed by means of GC/FID chromatography (3900, Varian) using a 25 m length and 0.32 mm i.d. capillary column (CP-FFAP CB, Varian) and nitrogen as carrier gas. Chloride ions concentration was determined by ionic chromatography (Metrohm IC25) using a 2 x 250 mm IonPak AG11-HC column and a 2 x 50 mm AS11-HC pre-column (Dionex).

3. Results and discussion

3.1. Characterization of the Pd/TiC-CDC catalysts

Fig. 1 shows the 77 K N_2 adsorption-desorption isotherms of the Pd/TiC-CDC catalysts. Two different trends can be clearly observed. The catalysts whose TiC-CDCs supports were produced at temperatures up to 1000 ºC are Type I according to the IUPAC classification, corresponding basically to microporous solids. Increasing the synthesis temperature led to more mesoporous materials, being the isotherms for Pd/TiC-CDC-1200 and Pd/TiC-CDC-1300 of type IV. The surface area, pore volume and mean pore size values obtained from those isotherms are collected in Table 1. As can be seen, the surface area slightly increased by increasing the extraction temperature from 800 to 1000 ºC whereas higher temperatures led to a remarkable surface decay. On the other hand, the pore volume was quite similar for the different samples whereas the mean pore size got broader with increasing extraction temperature (see Fig. S1 of the Supplementary Material for pore size distribution of the catalysts). These values are consistent with those reported for H_2SO_4-oxidized TiC-CDC materials in literature [27, 38]. Hasse et al. [27] showed that functionalization of TiC-CDC materials with sulfuric acid led to slight changes on their pore

structure and structural order, whereas nitric acid treatment collapsed partially the pore structure of the most amorphous TiC-CDCs tested (TiC-CDC-800). Accordingly, a low degree of functionalization was achieved with sulfuric acid and only low amounts of carboxylic and sulfonic groups were found. In line with the results obtained in the current work, those authors also concluded that subsequent deposition of the active phase and reduction do not affect significantly the TiC-CDC textural properties. On the other hand, the resulting Pd/TiC-CDC catalysts showed somehow basic PZC values, which are in the vicinity of those reported in previous works for Pd supported on AC catalysts [7, 26].

XRD and Raman spectroscopy were used to characterize the carbon microstructure of the Pd/Ti-CDC catalysts synthesized at different temperatures. Powder XRD data are collected in Fig. 2. TiC reflexes were not observed in any case, which allows confirming the absence of precursor residues in the carbon. It should also be noted that the peak associated with palladium was not observed in any of the patterns, mainly due to the high dispersion of palladium on the surface, consistently with the results obtained by cyclic voltammetry (Table 1). The range of the (002) and the (100) graphite planes (20-30º 2θ and 42-46º 2θ, respectively) provides information about the crystal height (L_c) and the crystal-width or in-plane size (L_a). For Pd/TiC-CDC-800 and Pd/TiC-CDC-1000, only a weak feature was observed for the (100) plane whereas it could not be seen for the (002) one, which is indicative of a highly amorphous structure. As expected, an increase in crystallinity with extraction temperature was achieved [27, 38]. In this sense, for Pd/TiC-CDC-1200 and Pd/TiC-CDC-1300 catalysts both (002) and (100) planes were clearly developed.

The Raman characterization is consistent with the XRD findings. The Raman spectra are depicted in Fig. 3a (see Fig. S2 of the Supplementary Material for peak deconvolution plots). All catalysts showed two shaped overlapping peaks in the first-order Raman spectrum characteristic of amorphous carbons [39, 40]. The disorder-induced D_1 band is located at ca. 1360 cm^{-1} and the graphitic band G_1 appears at ca. 1600 cm^{-1}, being their shoulder peaks referred as D_2 and G_2, respectively. On the other hand, only in the samples produced at extraction temperatures at or above 1200 ºC the S band, located at the second-order Raman spectrum and centered at 2700 cm^{-1} [39], was perceptibly seen. The full width at half

maximum (FWHM) of D_1 is sensitive for the degree of graphitization [27, 41] and the ratio of G_2 to G_1 band (I_{G2}/I_{G1}) is also related to the carbon structure as it is assumed to originate from sp^2 clusters with bond disorder due to four fold coordinated bonds [27, 40]. A decrease in FMWH and I_{G2}/I_{G1} ratio was found with increasing extraction temperature (Fig. 3b). Thus, the increase in degree of structural order of the Pd/Ti-CDC samples is clear, being also more evident the differences between Pd/TiC-CDC-800 and Pd/TiC-CDC-1000 than those previously observed by XRD. These results are in good agreement with previous works [27, 38].

3.2. Catalytic hydrodechlorination of 4-CP over Pd/TiC-CDCs in water

The application of carbon-supported catalysts in aqueous-phase HDC implies evaluating the adsorption capacity of the solid as the decay in the target pollutant concentration will likely be due both to adsorption onto the support and HDC reaction [26]. Therefore, the adsorption properties of the synthesized Pd/TiC-CDC catalysts were investigated prior developing the kinetic model which allows describing the whole sorption/HDC reaction system.

3.2.1. Adsorption properties

The influence of the textural properties of Pd/TiC-CDC catalysts was studied by independent adsorption equilibrium experiments in the absence of H_2 within the relevant concentration range where HDC experiments were performed. The adsorption isotherms of the main species involved in reaction (4-CP and Ph) onto the Pd/Ti-CDC catalysts synthesized at different temperatures are depicted in Fig. 4. These experimental data were successfully fitted by the usual Langmuir expression as follows:

$$C_{ADS_i} = \frac{K_{SORP_i} \cdot C_{ADS-MAX_i} \cdot C_{FREE_i}}{1 + K_{SORP_i} \cdot C_{FREE_i}} \quad (9)$$

i = 4-CP, Ph.

where C_{ADS} is the amount of 4-CP or Ph adsorbed on the catalyst at equilibrium; C_{FREE} is the equilibrium concentration of 4-CP or Ph in solution; K_{SORP} is the Langmuir adsorption equilibrium constant and $C_{ADS-MAX}$ is the maximum possible amount of solute adsorbed per unit mass of catalyst.

The calculated K_{SORP} and $C_{ADS-MAX}$ values are collected in Table 2. As expected, the specific surface area of the catalysts showed a strong effect on the adsorption capacity of the solid. In fact, as can be seen in Fig. 5, where the 4-CP maximum uptake is plotted versus the specific surface area of the catalysts, a linear relationship between both variables was found. Therefore, those catalysts showing the highest surface areas (Pd/TiC-CDC-800 and Pd/TiC-CDC-1000) exhibited the highest uptakes. On the other hand, the different crystallinity of the latter catalysts did not have any significant effect on their adsorption capacity, being their maximum uptakes almost the same. Thus, the effect of the structural order of the catalyst on its adsorption capacity did not seem to be crucial for the sorption behaviour of the solid with the catalysts tested in this work. The obtained maximum uptakes are in the vicinity of those previously reported in the literature using different commercial activated carbons [26]. In the same line, the K_{SORP} values of 4-CP were in all cases higher (up to 3 times) than those obtained for Ph, which is also consistent with previous contributions [26, 37].

3.2.2. HDC kinetics

Fig. 6 shows the evolution of 4-CP and the reaction products upon HDC with the Pd/TiC-CDC catalysts produced at different extraction temperatures. The obtained results are consistent with the consecutive reaction pathway previously reported for Pd-supported catalysts in which 4-CP reacts with hydrogen to produce Ph, which is further converted to C-one [12, 14]. As the removal of 4-CP is due to HDC but also to adsorption, both of them must be taken into account to deduce true kinetic constants and thus, compare the activity of the catalysts. In this sense, an expanded kinetic model based on the reaction pathway depicted in Scheme 1 and described in the experimental procedure was used to fit the experimental results [26] (Eqs. 2-7).

As can be seen in Fig. 6, the concentration profiles of the free reaction species resulting with all Pd/TiC-CDC catalysts were successfully fitted by the expanded kinetic model. Furthermore, it also allowed describing the evolution of the adsorbed organic compounds onto the TiC-CDC support (Fig. 6). According to the simulation, 4-CP was completely dechlorinated in all cases by the end of the experiment, being Ph the remaining adsorbed species. This assumption was confirmed by the experimental results as the amount of produced chloride ions at the end of reactions was above 95% of the initially added as 4-CP. Accordingly, the pH of the reaction medium was strongly reduced from the initial value (pH_0 = 6) to ~2.8. Therefore, the kinetic model allowed closing the carbon and chlorine balances during the whole reaction for all the Pd/TiC-CDC catalysts regardless of their sorption capacity.

The obtained HDC rate constants are collected in Table 3. As can be seen in Fig. 7, there is a trend between the sorption capacity of the TiC-CDC support and the resulting HDC rate. It seems clear that increasing the surface area of the support and thus the sorption capacity led to higher HDC rates, being Pd/TiC-CDC-800 and Pd/TiC-CDC-1000 catalysts the most active ones by far. Therefore, it can be concluded that a high surface density of 4-CP enhances significantly the HDC reaction. The Pd/TiC-CDC-1200 catalyst led to a HDC rate constant around 15 times lower than that obtained using Pd/TiC-CDC-1000. This difference cannot be explained exclusively by the lower surface area of the former (Table 1). Most probably, the difference in the structural order of both supports (Fig. 3) seems to play an additional role. It is reasonable that the higher structural order leads to an incomplete wetting of the catalyst, affecting the HDC rate. On the other hand, it needs to be noted that the HDC reaction is known to be structure sensitive [11, 42]. While the catalysts Pd/TiC-CDC-1000, Pd/TiC-CDC-1200 and Pd/TiC-CDC-1300 show a very similar Pd cluster size of ~5 nm, the cluster size for Pd/TiC-CDC-800 is smaller (2.8 nm). Thus, the reaction rate for Pd/TiC-CDC-800 should be intrinsically slightly smaller. However, due to the pronounced higher sorption capacity of the support, the reaction rate is higher than those shown by Pd/TiC-CDC-1200 and Pd/TiC-CDC-1300. The dependencies discussed are not affected by the differences on the cluster size, playing being the sorption capacity of the support the key role.

The mass specific activity of Pd/TiC-CDC catalysts was compared with those showed by commercial catalysts of high and low adsorption capacities (Pd/AC and Pd/Al_2O_3, respectively) tested in our previous work [26] (Fig. 8). As observed, the evolution of 4-CP upon reaction as well as the obtained HDC rate constants with Pd/Al_2O_3 were quite similar to those achieved with Pd/TiC-CDC-1200 and Pd/TiC-CDC-1300 catalysts. In the same line, the HDC rate constants of Pd/TiC-CDC-800 and Pd/TiC-CDC-1000 catalysts were remarkably higher than that obtained by Pd/AC catalyst, which can be directly attributed to the higher surface areas of the former ones. These findings impressively demonstrate the importance to tune the catalyst support and its sorption properties for the application in catalytic hydrodechlorination. The performance of the former Pd/TiC catalysts can be also favourably compared to a number of previously reported catalysts for the HDC of 4-CP under similar operating conditions. For the sake of comparison, the TOF values have been calculated (see Supporting Information for details) (Table 3). As representative examples, Molina et al. [14] obtained a TOF of 0.13 s^{-1} using an own-prepared Pd supported on pillared clay catalyst, Jin et al. [43] reported a TOF of 0.42 s^{-1} using a Pd supported on mesoporous silica-carbon nanocomposite and Xia et al. [44] showed a TOF of 0.42 s^{-1} with a Pd/C catalyst.

To further demonstrate the good performance of the catalysts prepared in this work, Pd/TiC-CDC-1000 was used at different operating temperatures (20 and 40 ºC) (see Fig. S3 of the Supplementary Material for experimental data). An activation energy of 21.7 kJ mol^{-1} for 4-CP conversion was obtained. This value is slightly lower than those previously reported for commercial Pd/AC catalysts (25-28 kJ mol^{-1}) [26] and significantly lower than those obtained with Pd-supported on pillared clays (39 kJ mol^{-1}) [14] and Al_2O_3 (47 kJ mol^{-1}) [10] catalysts.

3.3. Catalytic hydrodechlorination of 4-CP over Pd/TiC-CDCs in isopropanol

To get further insights on the effect of the sorption capacity of the catalytic support on the HDC kinetics, the sorption capacity was altered using the same supports but isopropanol as solvent. The

sorption capacity at the same operating conditions dropped more or less completely to zero when changing from aqueous to an isopropanol solution. This fact can be explained by the high affinity of 4-CP with the organic solvent, which favours that 4-CP molecules remain in solution instead of being adsorbed onto the carbon support [45]. Thus, when carrying out the HDC reaction in isopropanol matrix the influence of the support sorption capacity can be suppressed completely.

Fig. 9 shows the evolution of the reaction species upon HDC with the Pd/TiC-CDC catalysts using isopropanol as reaction solvent. These experimental data were successfully fitted by the kinetic model previously described; now taking into account that in this case adsorption can be neglected. Table 4 collects the obtained HDC rate constants. In accordance with previous works [46, 47], HDC rate constants were considerably lower than those obtained in water due to the lower polarity of the solvent. Nevertheless, the performance of Pd/ TiC-CDC catalysts was quite similar regardless their textural properties and even a slight increase on the HDC rate was observed by increasing the extraction temperature of the TiC-CDC support. These results contrast with those obtained using water as reaction solvent where the sorption capacity of the support was found to determine the HDC rates. Therefore, these findings validate that adsorption of organic compounds on carbon supports plays a key role on the HDC process in aqueous phase.

4. Conclusions

The use of well-defined TiC-CDCs synthesized at different extraction temperatures has proved to be an interesting approach for evaluating the effect of the catalytic support sorption capacity on the HDC process. We have found that a high surface density of 4-CP onto the catalyst surface enhances significantly the HDC reaction, a fact that so far remained unclear in the literature due to the scattering and low reproducible properties of conventional activated carbons. The optimum Pd/TiC-CDC-1000 catalyst has shown a very high activity in this process, achieving the complete conversion of 4-CP in 15 min reaction time at a HDC rate much higher than those previously reported for commercial Pd/AC

catalysts under similar operating conditions. The effect of the sorption process on the HDC performance has been further supported by the results obtained using isopropanol as solvent where sorption was suppressed and the activity of Pd/TiC-CDC catalysts did not depend on their specific surface area and/or degree of structural order. These results demonstrate the importance to tune the carbon support and its sorption properties for its application in aqueous-phase HDC.

Abbreviations

CDC: carbide-derived carbon

MPS: mean pore size

QSDFT: Quenched Solid Density Functional Theory

SPV: specific pore volume

SSA: specific surface area

TiC-CDC: titanium carbide-derived carbon

Acknowledgments

The authors gratefully acknowledge the funding of the German Research Council (DFG), which within the framework of its "Excellence Initiative" supports the Cluster of Excellence "Engineering of Advanced Materials" (www.eam.fau.de) at the University of Erlangen-Nuremberg.

Table and Figure captions

Table 1. Textural and surface properties of the Pd/TiC-CDC catalysts synthesized at different temperatures.

Table 2. Adsorption equilibrium data.

Table 3. Values of the HDC rate constants and TOF values with the Pd/TiC-CDC catalysts in aqueous phase.

Table 4. Values of the HDC rate constants with the Pd/ TiC-CDC catalysts using isopropanol as reaction solvent.

Scheme 1. HDC reaction pathway of 4-CP over Pd/TiC-CDC catalysts.

Fig. 1. N_2 adsorption-desorption isotherms at 77 K of the Pd/TiC-CDC catalysts synthesized at different temperatures within the range of 800-1300 ºC.

Fig. 2. XRD patterns of the Pd/TiC-CDC catalysts synthesized at different temperatures within the range of 800-1300 ºC.

Fig. 3. Raman analysis of the Pd/TiC-CDC catalysts synthesized at different temperatures within the range of 800-1300 ºC. a: Raman spectra. b: Full width at half maximum (FWHM) of D_1 band and ratio of I_{G2}/I_{G1} band.

Fig. 4. Experimental data (symbols) and Langmuir fits (solid lines) for the adsorption equilibrium of 4-CP and Ph onto the four different Pd/TiC-CDC catalysts at 30 ºC.

Fig. 5. Linear dependence of the maximum uptake of 4-CP on the specific surface area of the Pd/TiC-CDC catalyst.

Fig. 6. Time evolution of 4-CP (■), Ph (●) and C-one (▲) in the bulk phase with Pd/TiC-CDC catalysts synthesized at 800 (a), 1000 (b), 1200 (c) and 1300 (d). Experimental (symbols) and model fit (solid lines: free species, dash lines: adsorbed species).

Fig. 7. Dependence of the HDC rate constants on the sorption capacity of the Pd/TiC-CDC catalysts.

Fig. 8. Time evolution of 4-CP in the bulk phase with Pd/TiC-CDC catalysts synthesized at different temperatures and the commercial catalysts Pd/Al_2O_3 and Pd/AC [26] (a). HDC rate constants obtained with those catalysts (b).

Fig. 9. Time evolution of 4-CP (■), Ph (●) and C-one (▲) in the bulk phase (isopropanol) with Pd/TiC-CDC catalysts synthesized at 800 (a), 1000 (b), 1200 (c) and 1300 (d). Experimental (symbols) and model fit (solid lines).

References

[1] F.J. Urbano, J.M. Marinas, J. Mol. Catal. 173 (2001) 329–345.

[2] P. Lampi, T. Vartiainen, J. Toumisto, A. Hesso, Chemosphere 20 (1990) 625–634.

[3] M. Czaplicka, Sci. Total Environ. 322 (2004) 21–39.

[4] Y. Persson, A. Shchukarev, L. Öberg, M. Tysklind, Environ. Sci. Pollut. Res. 15 (2008) 463–471.

[5] M.J. Gómez, S. Herrera, D. Solé, E. García-Calvo, A.R. Fernández-Alba, Anal. Chem. 83 (2011) 2638–2647.

[6] M.A. Keane, ChemCatChem 3 (2011) 800–821.

[7] G. Yuan, M.A. Keane, Appl. Catal., B 52 (2004) 301–314.

[8] M.A. Keane, Appl. Catal., A 271 (2004) 109–118.

[9] M.A. Keane, G. Pina, G. Tavoularis, Appl. Catal., B 48 (2004) 275–286.

[10] E. Díaz, J.A. Casas, A.F. Mohedano, L. Calvo, M.A. Gilarranz, J.J. Rodriguez, Ind. Eng. Chem. Res. 47 (2008) 3840–3846.

[11] J.A. Baeza, L. Calvo, M.A. Gilarranz, A.F. Mohedano, J.A. Casas, J.J. Rodriguez, J. Catal. 293 (2012) 85–93.

[12] M. Munoz, Z.M. de Pedro, J.A. Casas, J.J. Rodriguez, Appl. Catal., A 488 (2014) 78–85.

[13] J.A. Baeza, L. Calvo, M.A. Gilarranz, J.J. Rodriguez, Chem. Eng. J. 240 (2014) 271–280.

[14] C.B. Molina, A.H. Pizarro, J.A. Casas, J.J. Rodriguez, Appl. Catal., B 148–149 (2014) 330–338.

[15] E.V. Golubina, E.S. Lokteva, S.A. Kachevsky, A.O. Turakulova, V.V. Lunin, Stud. Surf. Sci. Catal. 175 (2010) 293–296.

[16] S. Gómez-Quero, F. Cárdenas-Lizana, M.A. Keane, Ind. Eng. Chem. Res. 47 (2008) 6841–6853.

[17] S.C. Shekhar, J.K. Murthy, P.K. Rao, K.S.R. Rao, Appl. Catal., A 271 (2004) 95–101.

[18] L. Calvo, M.A. Gilarranz, J.A. Casas, A.F. Mohedano, J.J. Rodriguez, Appl. Catal., B. 67 (2006) 68–76.

[19] E. Diaz, A.F. Mohedano, J.A. Casas, L. Calvo, M.A. Gilarranz, J.J. Rodriguez, Appl. Catal., B 106 (2011) 469–475.

[20] J.A. Baeza, L. Calvo, J.J. Rodriguez, M.A. Gilarranz, Chem. Eng. J. 294 (2016) 40–48.

[21] A. Gil, G. Puente, P. Grange, Microporous Mater. 12 (1997) 51–61.

[22] L. Calvo, M.A. Gilarranz, J.A. Casas, A.F. Mohedano, J.J. Rodriguez, Ind. Eng. Chem. Res. 44 (2005) 6661–6667.

[23] Suhas, P.J.M. Carrott, M.M.L. Ribeiro Carrott, Bioresour. Technol. 98 (2007) 2301–2312.

[24] A. Demirbas, J. Hazard. Mater. 167 (2009) 1–9.

[25] J.M. Dias, M.C.M. Alvim-Ferraz, M.F. Almeida, J. Rivera-Utrilla, M. Sánchez-Polo, J. Environ. Manage. 85 (2007) 833–846.

[26] M. Munoz, M. Kaspereit, B.J.M. Etzold, Chem. Eng. J. 285 (2016) 228–235.

[27] B. Hasse, J. Gläsel, A.M. Kern, D.Y. Murzin, B.J.M. Etzold, Catal. Today 249 (2015) 30–37.

[28] R.K. Dash, G. Yushin, Y. Gogotsi, Microporous Mesoporous Mater. 86 (2005) 50–57.

[29] V. Presser, M. Heon, Y. Gogotsi, Adv. Funct. Mater. 21 (2011) 810–833.

[30] A. Silvestre-Albero, S. Rico-Francés, F. Rodríguez-Reinoso, A.M. Kern, M. Klumpp, B.J.M. Etzold, J. Silvestre-Albero, Carbon 59 (2013) 221–228.

[31] J. Gläsel, J. Diao, Z. Feng, M. Hilgart, T. Wolker, D.S. Su, B.J.M. Etzold, Chem. Mater. 27 (2015) 5719–5725.

[32] T. Knorr, A. Schwarz, B.J.M. Etzold, Chem. Eng. Technol. 37 (2014) 453–461.

[33] A.V. Kirilin, B. Hasse, A.V. Tokarev, L.M. Kustov, G.N. Baeva, G.O. Bragina, A.Y. Stakheev, A. Rautio, T. Salmi, B.J.M. Etzold, J. Mikkola, D.Y. Murzin, Catal. Sci. Technol. 4 (2014) 387–401.

[34] L. Borchardt, F. Hasché, M.R. Lohe, M. Oschatz, F. Schmidt, E. Kockrick, C. Ziegler, T. Lescouet, A. Bachmatiuk, B. Büchner, D. Farrusseng, P. Strasser, S. Kaskel, Carbon 50 (2012) 1861–1870.

[35] F. Glenk, T. Knorr, M. Schirmer, S. Gütlein, B.J.M. Etzold, Chem. Eng. Technol. 33 (2010) 698–703.

[36] Y. Zhou, Z. Li, X. Pan, X. Bao, J. Mater. Chem. 22 (2012) 14155–14159.

[37] Yu. Shindler, Yu. Matatov-Meytal, M. Sheintuch, Ind. Eng. Chem. Res. 40 (2001) 3301–3308.

[38] R. Dash, J. Chmiola, G. Yushin, Y. Gogotsi, G. Laudisio, J. Singer, J. Fischer, S. Kucheyev, Carbon. 44 (2006) 2489–2497.

[39] P. Lespade, A. Marchand, M. Couzi, F. Cruege, Carbon. 22 (1984) 375–385.

[40] N. Shimodaira, A. Masui, J. Appl. Phys. 92 (2002) 902–909.

[41] S. Osswald, E. Flahaut, H. Ye, Y. Gogotsi, Chem. Phys. Lett. 402 (2005) 422–427.

[42] L.M. Gomez-Sainero, X.L. Seoane, J.L.G. Fierro, A. Arcoya, J. Catal. 209 (2002) 279-288.

[43] Z. Jin, C. Yu, X. Wang, Y. Wan, D. Li, G. Lu, Chem. Commun. (2009) 4438–4440.

[44] C. Xia, Y. Liu, S. Zhou, C. Yang, S. Liu, J. Xu, J. Yu, J. Chen, X. Liang, J. Hazard. Mater. 169 (2009) 1029–1033.

[45] B. Cabal, C.O. Ania, J.B. Parra, J.J. Pis, Chemosphere 76 (2009) 433–438.

[46] S. Gómez-Quero, F. Cárdenas-Lizana, M.A. Keane, AIChE J. 56 (2010) 756–767.

[47] X. Ma, Y. Liu, X. Li, J. Xu, G. Gu, C. Xia, Appl. Catal., B 165 (2015) 351–359.

Table 1

	SSA (m^2 g^{-1})	**SPV (cm^3 g^{-1})**	**MPS (nm)**	**Pd dispersion (%)**	**PZC**
Pd/ TiC-CDC-800	1519	0.76	0.87	40.8	7.3
Pd/ TiC-CDC-1000	1589	0.71	0.89	27.0	8.1
Pd/ TiC-CDC-1200	1159	0.75	1.29	21.6	9.7
Pd/ TiC-CDC-1300	564	0.70	2.49	20.3	9.8

Table 2

	4-CP			Ph		
	K_{SORP} (L $mmol^{-1}$)	$C_{ADS-MAX}$ (mmol g_{cat}^{-1})	R^2	K_{SORP} (L $mmol^{-1}$)	$C_{ADS-MAX}$ (mmol g_{cat}^{-1})	R^2
Pd/TiC-CDC-800	21.2	2.5	0.99	6.4	2.3	0.99
Pd/TiC-CDC-1000	18.7	2.6	0.99	8.6	2.4	0.99
Pd/TiC-CDC-1200	6.0	1.7	0.99	2.6	2.0	0.99
Pd/TiC-CDC-1300	4.7	0.8	0.99	1.5	0.9	0.99

Table 3

Catalyst	k_{HDC-1} x 10^3 (L $mg_{Pd\ surf}^{-1}$ s^{-1})	k_{HDC-2} x 10^5 (L $mg_{Pd\ surf}^{-1}$ s^{-1})	R^2	TOF_{HDC-1} (s^{-1})
Pd/TiC-CDC-800	4.90	0.27	0.99	1.52
Pd/TiC-CDC-1000	15.1	0.48	0.99	4.70
Pd/TiC-CDC-1200	0.93	0.65	0.98	0.33
Pd/TiC-CDC-1300	0.49	1.60	0.98	0.15

Table 4

Catalyst	k_{HDC-1} x 10^5 (L $mg_{Pd\ surf}^{-1}$ s^{-1})	k_{HDC-2} x 10^5 (L $mg_{Pd\ surf}^{-1}$ s^{-1})	R^2
Pd/TiC-CDC-800	1.35	0.34	0.99
Pd/TiC-CDC-1000	2.26	0.37	0.98
Pd/TiC-CDC-1200	3.24	0.42	0.99
Pd/TiC-CDC-1300	3.89	0.44	0.98

Figure 1 revised

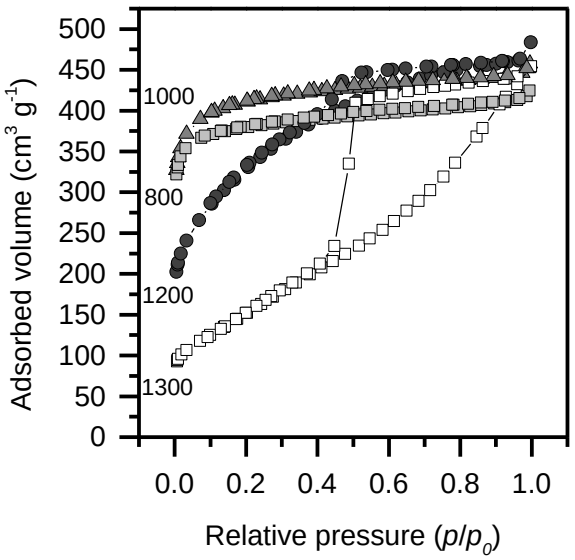

Figure 2

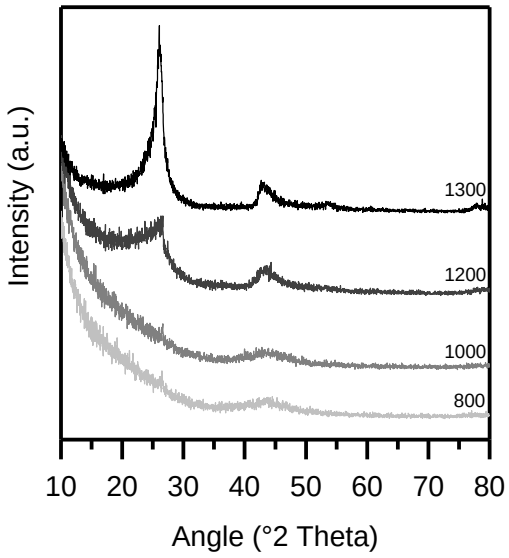

Figure 3

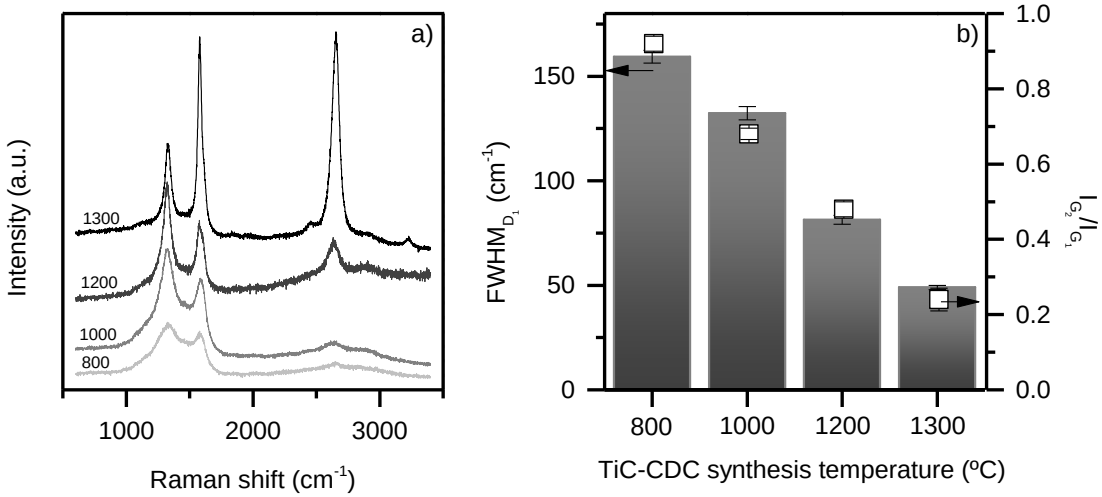

Figure 4

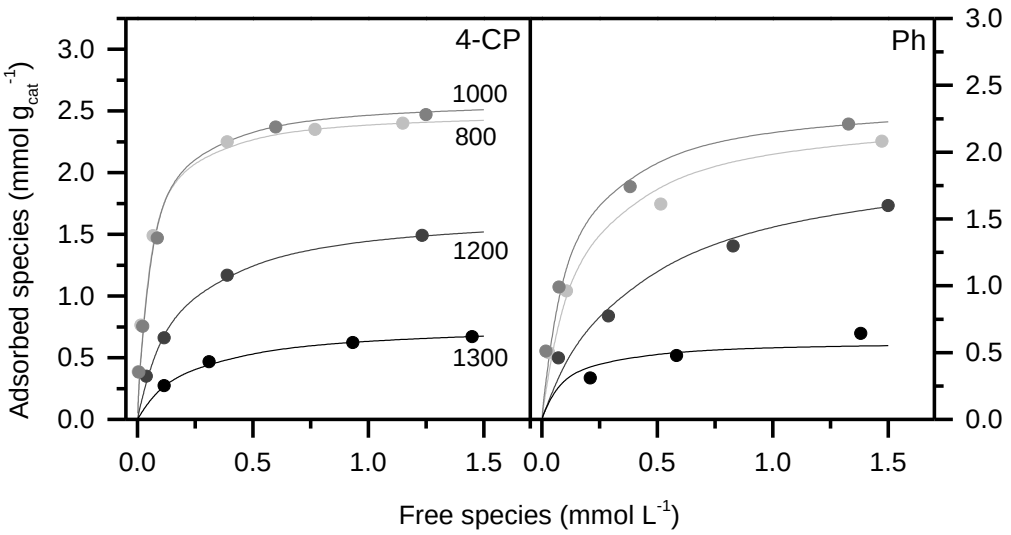

Figure 5

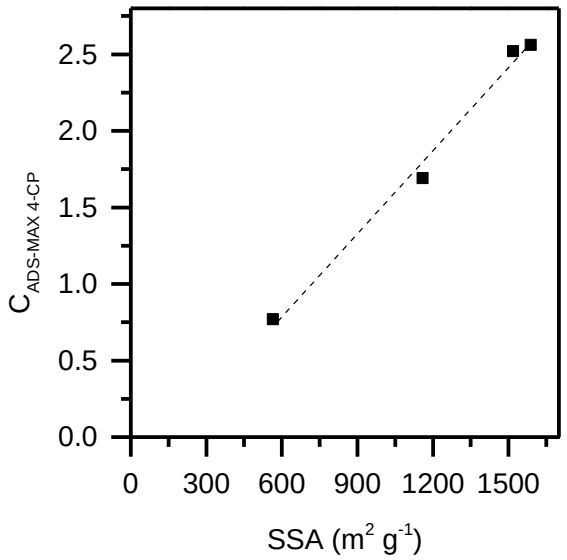

Figure 6

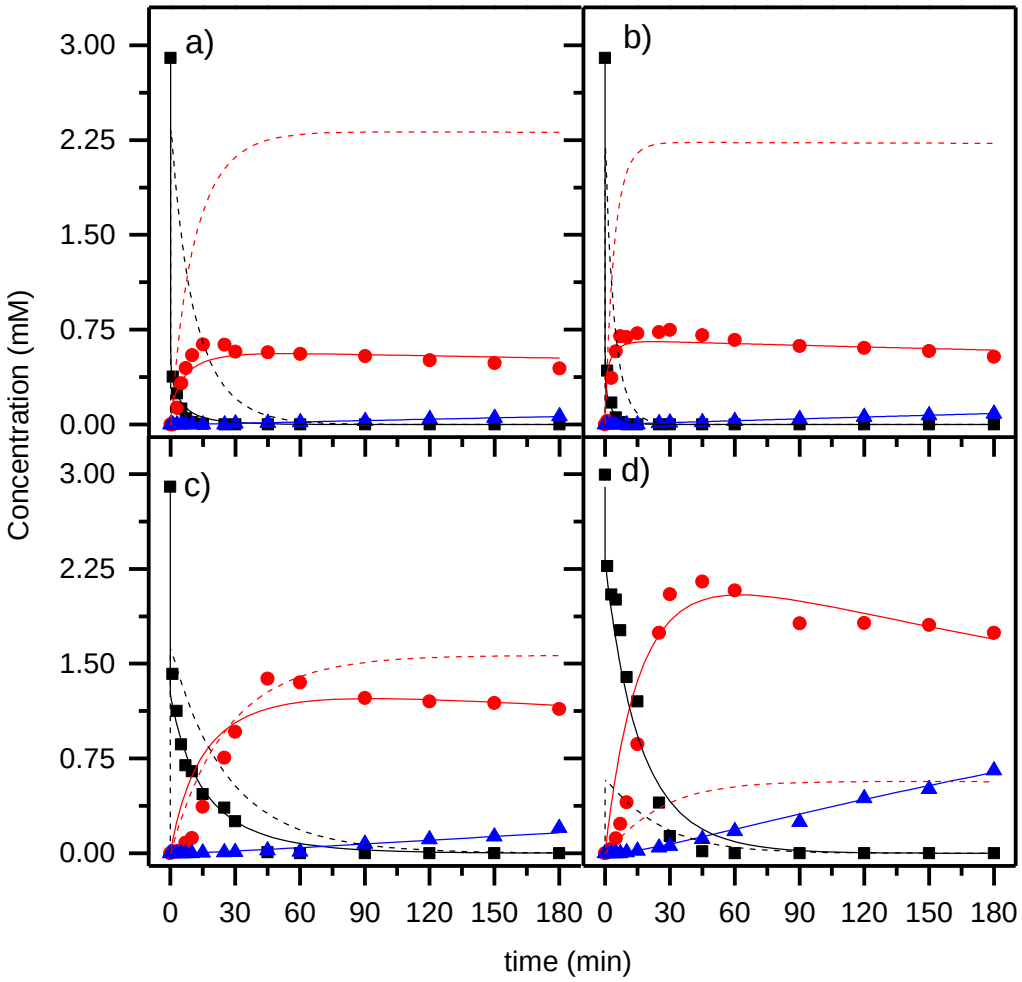
a)
b)
c)
d)
Concentration (mM)
time (min)
3.00
2.25
1.50
0.75
0.00
0
30
60
90
120
150
180

Figure 7

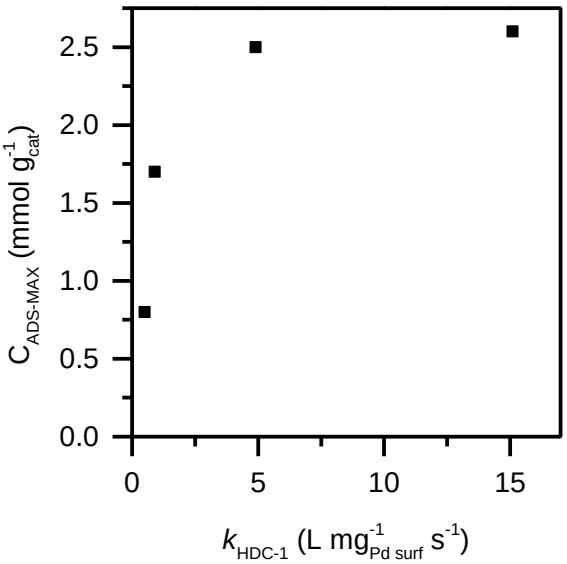
$C_{ADS-MAX}$ (mmol g_{cat}^{-1})
k_{HDC-1} (L $mg_{Pd\ surf}^{-1}$ s^{-1})
2.5
2.0
1.5
1.0
0.5
0.0
0
5
10
15

Figure 8

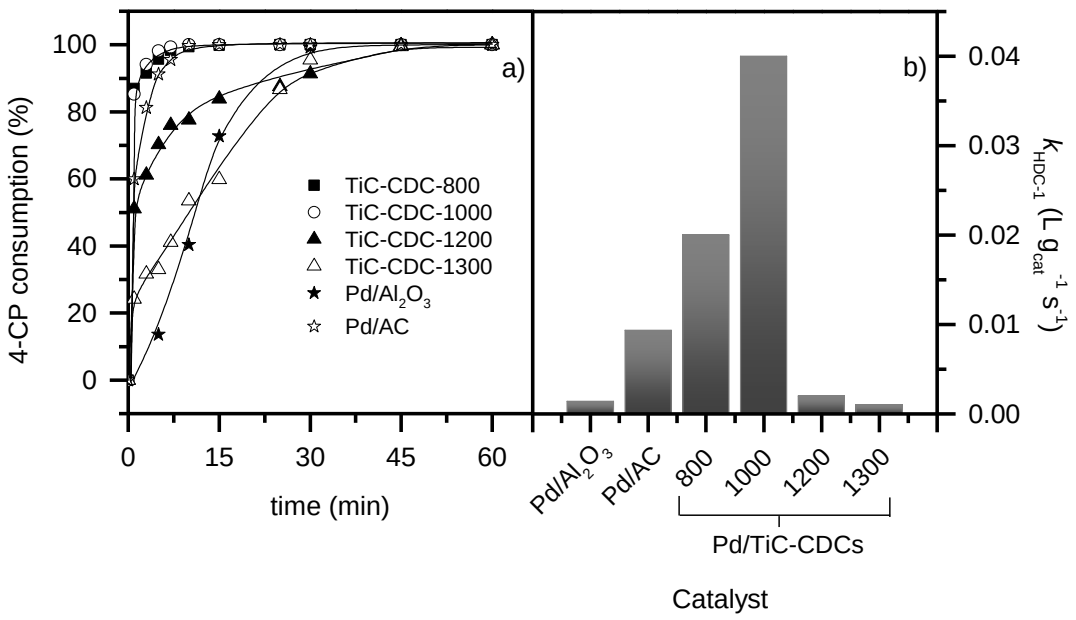

Figure 9

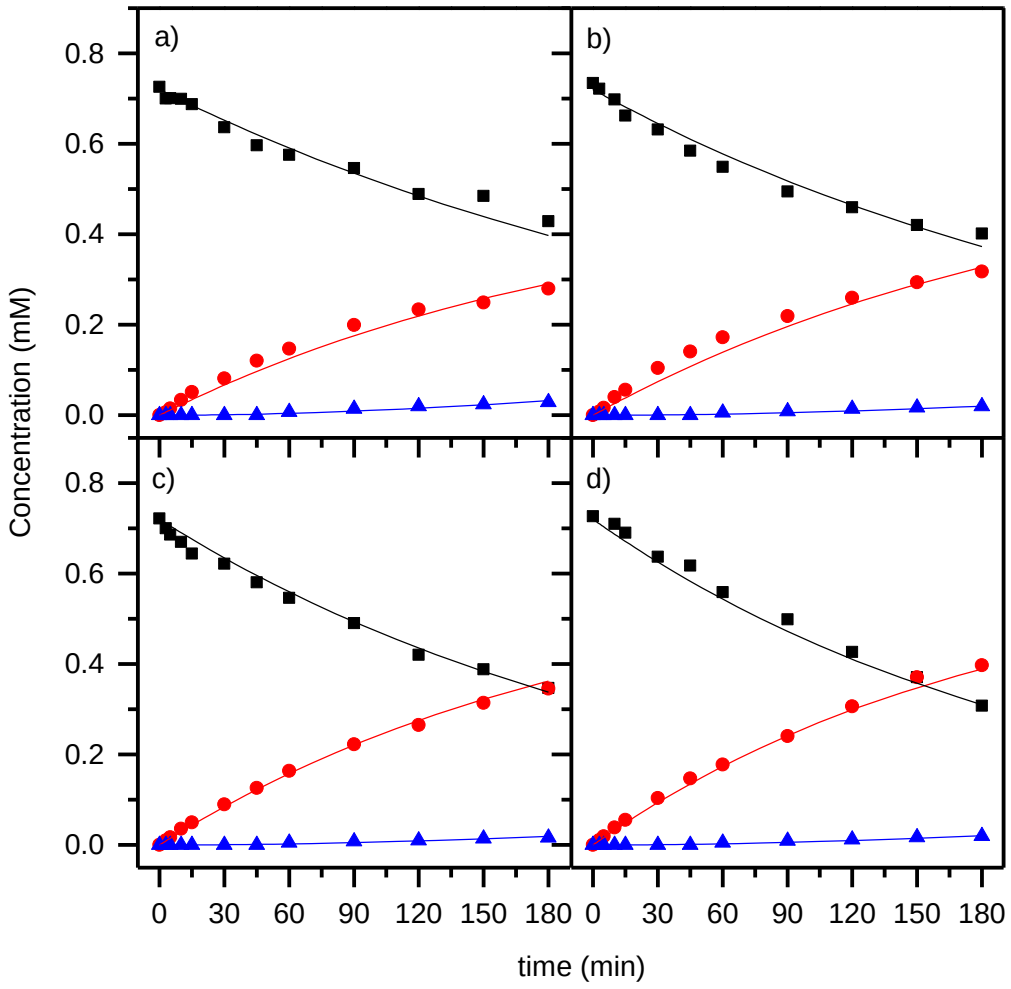
a)
b)
c)
d)
Concentration (mM)
time (min)
0.0
0.2
0.4
0.6
0.8
0
30
60
90
120
150
180

Scheme 1

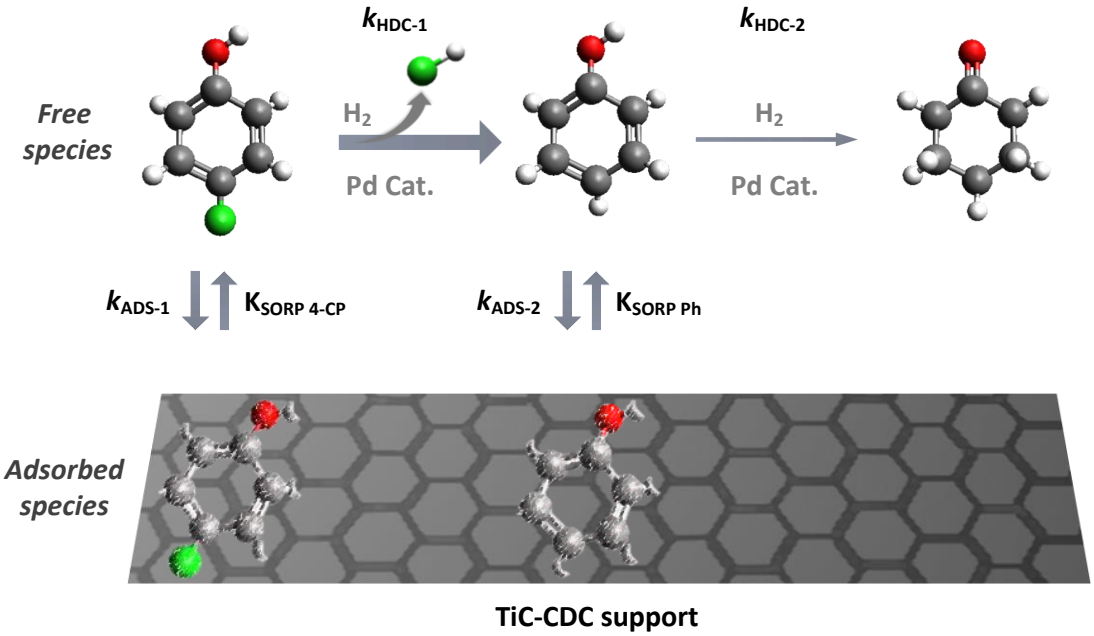
Free species
k_{HDC-1}
H_2
Pd Cat.
k_{HDC-2}
H_2
Pd Cat.
k_{ADS-1}
$K_{SORP\ 4\text{-}CP}$
k_{ADS-2}
$K_{SORP\ Ph}$
Adsorbed species
TiC-CDC support